PAPER

Check for updates

Gold nanoparticles decorated with monosaccharides and sulfated ligands as potential modulators of the lysosomal enzyme *N*-acetylgalactosamine-6-sulfatase (GALNS)†

Francesca Buco, [a] Camilla Matassini, *[a] Costanza Vanni,[a] Francesca Clemente, [a] Paolo Paoli, [b] Cosimo Carozzini,[a] Alice Beni,[a] Francesca Cardona, [a] Andrea Goti, [a] Sergio Enrique Moya, [c] Maria Grazia Ortore, [d] Patrizia Andreozzi,[a] Amelia Morrone[e,f] and Marco Marradi *[a]

N-Acetylgalactosamine-6-sulfatase (GALNS) is an enzyme whose deficiency is related to the lysosomal storage disease Morquio A. For the development of effective therapeutic approaches against this disease, the design of suitable enzyme enhancers (*i.e.* pharmacological chaperones) is fundamental. The natural substrates of GALNS are the glycosaminoglycans keratan sulfate and chondroitin 6-sulfate, which mainly display repeating units of sulfated carbohydrates. With a biomimetic approach, gold nanoparticles (AuNPs) decorated with simple monosaccharides, sulfated ligands (homoligand AuNPs), or both monosaccharides and sulfated ligands (mixed-ligand AuNPs) were designed here as multivalent inhibitors of GALNS. Among the homoligand AuNPs, the most effective inhibitors of GALNS activity are the β-D-galactoside-coated AuNPs. In the case of mixed-ligand AuNPs, β-D-galactosides/sulfated ligands do not show better inhibition than the β-D-galactoside-coated AuNPs. However, a synergistic effect is observed for α-D-mannosides in a mixed-ligand coating with sulfated ligands that reduced IC$_{50}$ by one order of magnitude with respect to the homoligand α-D-mannoside-coated AuNPs. SAXS experiments corroborated the association of GALNS with β-D-galactoside AuNPs. These AuNPs are able to restore the enzyme activity by almost 2-fold after thermal denaturation, indicating a potential chaperoning activity towards GALNS. This information could be exploited for future development of nanomedicines for Morquio A. The recent implications of GALNS in cancer and neuropathic pain make these kinds of multivalent bionanomaterials of great interest towards multiple therapies.

[a]Department of Chemistry 'Ugo Schiff', University of Firenze, via della Lastruccia 13, Sesto Fiorentino, FI, Italy. E-mail: marco.marradi@unifi.it, camilla.matassini@unifi.it

[b]Department of Experimental and Clinical Biomedical Sciences, University of Florence, Viale Morgagni 50, 50134 Firenze, Italy

[c]CIC biomaGUNE, Basque Research and Technology Alliance (BRTA), Paseo Miramon 182 C, Donostia-San Sebastián 20014, Spain

[d]Department of Life and Environmental Sciences, Marche Polytechnic University, Via Brecce Bianche, Ancona, I-60130, Italy

[e]Laboratory of Molecular Biology of Neurometabolic Diseases, Meyer Children's Hospital, IRCCS, Viale Pieraccini 24, 50139, Firenze, Italy

[f]Department of Neurosciences, Psychology, Drug Research and Child Health, University of Florence, Viale Pieraccini 24, 50139 Firenze, Italy

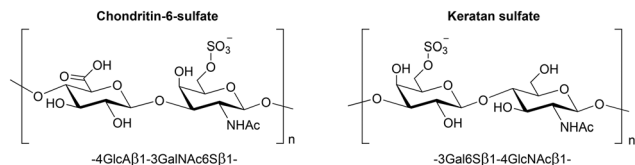†Electronic supplementary information (ESI) available. See DOI: https://doi.org/10.1039/d3ob01466e

Introduction

Lysosomal Storage Disorders (LSDs) are metabolic diseases caused by enzyme misfolding or deficiency that leads to accumulation of unmetabolized substrates in the lysosomes.[1] Although LSDs are individually considered as rare pathologies, they collectively affect 1 in 5000 live births. The use of mimetics of natural substrates that can behave as pharmacological chaperones (PCs)[2] is important to develop new therapies for LSDs. PCs are compounds that can specifically bind and stabilize a protein or restore its lost functionality.[3] For example, the drug Migalastat (deoxygalactonojirimycin, Galafold®), recently approved by the EMA and FDA, is able to restore the functionality of α-galactosidase A whose malfunction causes Fabry disease.[4]

Among LSDs, Morquio A syndrome (also known as Mucopolysaccharidosis IVA)[5] is a rare disease related to the deficiency of the lysosomal enzyme *N*-acetylgalactosamine-6-sulfatase (GALNS), whose natural substrates are the glycosaminoglycans (GAGs) keratan sulfate and chondroitin 6-sulfate (Fig. 1).[6]

Morquio A is currently treated by enzyme replacement therapy (ERT), namely, by infusion of the orphan medicine

Fig. 1 Natural substrates of the GALNS enzyme: the GAGs chondroitin-6-sulfate and keratan sulfate.
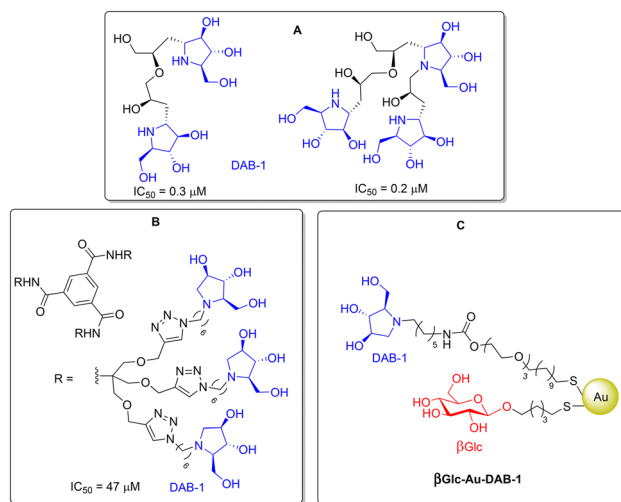
Fig. 2 Multivalent inhibitors of the GALNS enzyme: iminosugar DAB-1 dimers or trimers (A), dendrimers (B) and βGlc-AuNPs decorated with DAB-1 (C).

VIMIZIM® (elosulfase alfa, BioMarin),[7] which is based on recombinant human GALNS (rhGALNS). However, rhGALNS suffers from low stability *in vivo*; thus, a way to improve this ERT could be to chaperone the enzyme infusion with a stabiliser. This is the so-called PC/ERT combined therapy and has been experimented for other LSDs.[8] This approach would reduce the dose of the infused enzyme and the administration frequency, greatly benefitting the patients' quality of life. The identification of rhGALNS inhibitors is the starting point for the development of enzyme stabilizers towards this aim.[2c]

Recently, a repurposing study based on molecular docking virtual screenings identified the small molecules ezetimibe and pranlukast,[9] and bromocriptine[10] as PCs for the treatment of Morquio A, thus highlighting the importance of finding new molecules to treat mucopolysaccharidoses.[11]

Moreover, recent reports highlighted the implications of GALNS not only in LSDs but also in cancer[12] and neuropathic pain.[13] The three-dimensional structure of human GALNS, determined by X-ray crystallography at 2.2 Å resolution, shows that the enzyme is a dimer.[14] In the last few years, it has been demonstrated that in addition to carbohydrate-binding proteins (lectins),[15] carbohydrate-processing enzymes[16] may also benefit from polyvalent interactions that can occur through the binding of multiple ligands with multiple receptors.[17]

The dimeric nature of GALNS led to the hypothesis that the interaction of GALNS with the corresponding ligands could take advantage of the "multivalent" display of carbohydrates and/or sulfate esters, which are the repetitive moieties found in the enzyme's natural substrates chondroitin-6-sulfate and keratan sulfate (Fig. 1).

The multimerization of the iminosugar 1,4-dideoxy-1,4-imino-D-arabinitol (DAB-1) in a dimeric or trimeric form[18] on dendrimeric scaffolds[19] or on gold nanoparticles (AuNPs)[20] (Fig. 2) resulted in new multivalent systems that efficiently inhibit GALNS (low micromolar range). Indeed, iminosugars,[21] which are well-known carbohydrate mimics, were initially selected as ligands for their measurable chaperoning activities towards lysosomal enzymes.[2b]

Surprisingly, good inhibition was also obtained with AuNPs coated with β-D-glucosides (Fig. 3, AuNPs **1**),[20] which could be explained by the low specificity of the GALNS substrate-binding pocket. Such enzyme promiscuity was already noted in the original report by Garman and co-workers.[14]

In light of the latter result, and with the aim to collect more information on the interaction between GALNS and multivalent systems, we reasoned that glyco-AuNPs decorated with monosaccharides other than glucose could also work as new inhibitors of GALNS. Glyco-AuNPs are designed to display sugars on a nanometric gold core in a polyvalent and globular arrangement and with a well-defined chemical composition. They are easily prepared through *in situ* reduction of Au(III) salts in the presence of a suitable thiol-ended glycoside, thus providing valuable tools to study and intervene in carbohydrate-mediated interactions.[22]

In the present article, a series of homoligand glyco-AuNPs (AuNPs **1–4**, Fig. 3, top), *i.e.* nanoparticles decorated with thiol-ending α-D-mannosides or α- or β-D-galactosides, were prepared and tested as GALNS inhibitors, integrating the results obtained with AuNPs coated with β-D-glucosides.[20] The main goal of this work was to study if the nature of the sugar (*e.g.* glucose, mannose or galactose) and the type of glycosidic linkage (*e.g.* α- or β-anomeric configuration) could affect the inhibition. Furthermore, with a minimalist approach, mixed-ligand AuNPs simultaneously decorated with these glycosides and sulfate-ending ligands (AuNPs **7–10**, Fig. 3, bottom) were also designed and prepared to include the sulfate moiety present in the natural GAG substrates of GALNS (Fig. 1).

AuNPs are ideal scaffolds to obtain a mixed functionalization of nanosystems; indeed, once the thiol-ending ligands are in hand, AuNPs allow for a straightforward modulation of the multivalent ligand presentation by tuning the percentage of each ligand on the gold surface simply by mixing the ligands together before the reduction step. Inhibition assays of the so-prepared AuNPs were performed *in vitro*. The best inhibitor was tested as an rhGALNS stabiliser and monitored in solution by small angle X-ray scattering (SAXS) measurements in the presence and absence of GALNS in order to get an insight into the NP–enzyme interaction.
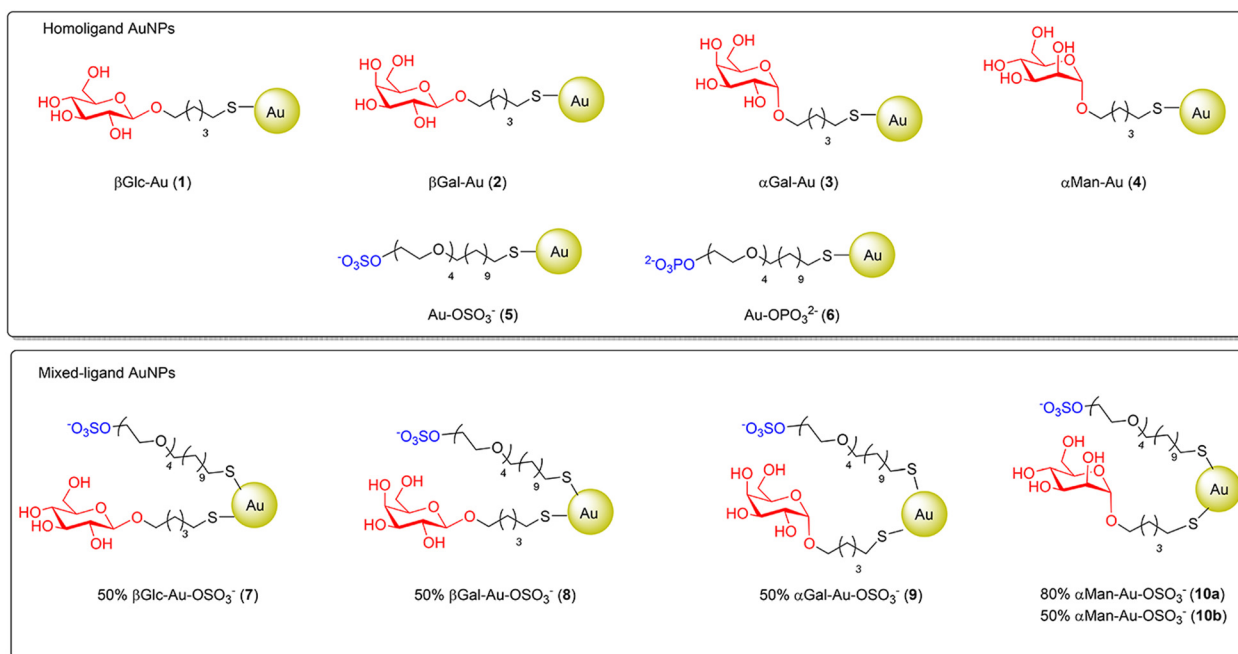
Fig. 3 The whole set of prepared AuNPs. Homoligand AuNPs (top) (100% sugar, 100% sulfate, or 100% phosphate) and mixed-ligand AuNPs (bottom) (percentage indicates the sugar content with respect to the sulfated ligand).

Results and discussion

Preparation of homoligand AuNPs

First, a battery of AuNPs decorated with thiol-ending glycosides or negatively charged ligands (sulfate and phosphate derivatives) was prepared (homoligand AuNPs, Fig. 3, top).

The preparation of the 100% glyco-AuNPs **1–4** was carried out following the method of Penadés and collaborators[23] inspired by the Brust and Schiffrin synthesis[24] (for details, see the ESI†). The protocol involves the use of suitable thiol-ending glycosides as ligands for the functionalisation of the surface of gold nanoparticles, which are formed *in situ* through reduction of $HAuCl_4$ with an excess of sodium borohydride. In particular, the 100% glyco-AuNPs **1–4** were synthesized using suitable thiol-ending glycosides with a linear aliphatic linker bearing five carbon atoms, following established procedures.[25]

In addition, AuNPs **5** coated with a sulfated ligand were also prepared as reported in the literature.[26] The sulfated ligand consists of a part of tetra(ethylene glycol) (TEG) and a linear aliphatic chain made up of eleven carbon atoms. The long aliphatic chain guarantees the formation of self-assembled monolayers (SAMs) on the gold surface, while the TEG component guarantees flexibility, promotes solubility in water and prevents non-specific adsorption of other biomolecules (*e.g.* proteins). A phosphate analogue was also synthesised to prepare the corresponding AuNPs **6** as a negatively charged control system.

Preparation of mixed-ligand AuNPs

The possibility to tailor more than one ligand on the same AuNPs allowed for the generation of AuNPs **7–10** (Fig. 3 bottom), which display a 1:1 mixture of a sugar component

(also a 4:1 mixture in the case of mannosides; see below) and the sulfated ligand. In analogy to the already reported AuNPs **7**,[26] AuNPs **8–10** were prepared by mixing the sulfated ligand *in situ* with one of the thiol-ending glycosides glycoC5S in the appropriate ratio (see Table 1 and Fig. 3) in a 3:3:1 H_2O/CH_3OH/CH_3COOH solvent mixture. An aqueous $HAuCl_4$ solution was added to this ligand mixture (overall 3 equiv. with respect to gold), and the resulting solution was treated with an excess of $NaBH_4$ and vigorously stirred for 2 hours at room temperature. After evaporation of the solvent, the AuNPs were washed with methanol. The residue was dispersed in Milli-Q water and purified by dialysis against water. After freeze-drying, the AuNPs were re-dispersible in water. Analogously to homoligand AuNPs, the mixed-ligand AuNPs showed an exceptionally small core (most in the 1–2 nm range), as demonstrated by TEM and UV-vis analyses. TEM micrographs showed uniform dispersion of the Au-NPs and no aggregation was evident. In agreement with TEM data, no well-defined plasmon absorption maximum (at around 520 nm), typical of AuNPs with larger gold diameters, was observed for these AuNPs. All of the obtained AuNPs are water dispersible and are stable for months (no flocculation) under physiological conditions at room temperature. Based on the gold core size (determined by TEM), the average number of gold atoms per nanoparticle was calculated according to Murray's data that also provide an estimation of the gold surface atoms.[27] The latter number sets an approximate limit of organic ligands that can be anchored onto the AuNP surface. The combination of this information with the elemental analysis experimental values allows for estimating the number of ligands anchored to the gold surface, from which an average molecular formula

9364 | *Org. Biomol. Chem.*, 2023, **21**, 9362–9371

This journal is © The Royal Society of Chemistry 2023

Table 1 Percentage of inhibition of AuNPs towards human GALNS from leukocyte homogenate. IC$_{50}$ values were measured for inhibition percentage higher than 70%

AuNP	Ligand composition	% GALNS inhibition[a] (0.2 mg mL^{-1})	IC$_{50}$ (µg mL^{-1})[a]	IC$_{50}$[b] (µM)
1	100% βGlc	75[c]	28[c]	47
2	100% βGal	92	9 ± 2 (6 ± 1)[d]	11 (7)[d]
3	100% αGal	86	140 ± 10	194
4	100% αMan	92	120 ± 4	175
5	100% OSO$_3^-$	42	—	—
6	100% OPO$_3^{2-}$	27	—	—
7	50% βGlc 50% OSO$_3^-$	86	120 ± 10	84
8	50% βGal 50% OSO$_3^-$	88	23 ± 2	9
9	50% αGal 50% OSO$_3^-$	58	—	—
10a	80% αMan 20% OSO$_3^-$	93	50 ± 8	46
10b	50% αMan 50% OSO$_3^-$	94	15 ± 2	7
βGlc-Au-DAB-1	60% βGlc 40% DAB-1	88[c]	16[c]	2.51[c,e]

[a] AuNP concentration. [b] Sugar concentration. [c] Taken from ref. 20. [d] The values in brackets refer to the commercially available drug VIMIZIM® (rhGALNS). [e] Iminosugar concentration.

can be derived for each functionalized AuNP. The amount of sulfated ligand was confirmed by quantitative ^{1}H NMR (qNMR) in D$_2$O using 3-(trimethylsilyl)propionic-2,2,3,3-d4 acid (TSP-d4) as an internal reference.[20,28] A representative example of characterization is shown in Fig. 4 for AuNPs **8**.

AuNPs as multivalent inhibitors of GALNS

The screening of inhibitors, as anticipated, is the starting point to find potential PC-like systems, which can stabilise the

Fig. 4 Characterization of 50% βGal-Au-OSO$_3^-$ (**8**): (A) TEM micrograph; (B) size-distribution histogram obtained by measuring 300 nanoparticles (average diameter 1.2 ± 0.4 nm); (C) UV-vis spectrum in H$_2$O (0.2 mg mL^{-1}); (D) q^{1}H NMR (400 MHz) in D$_2$O containing 0.05 wt% of 3-(trimethylsilyl)propionic-2,2,3,3-d$_4$ acid, sodium salt as the internal standard.

infused rhGALNS currently used in therapy. In a previous work,[20] it was observed that gold nanoparticles decorated with 100% βGlc (AuNPs **1**, Fig. 3) showed remarkable inhibition towards GALNS (75% inhibition at 0.2 mg mL^{-1}, IC$_{50}$ = 0.028 mg mL^{-1}, corresponding to 47 µM in terms of glucose; see Table 1). Conversely, neither the monovalent thiol-ending glucoside βGlcC$_5$SH nor its divalent disulfide (βGlcC$_5$S)$_2$ showed inhibitory activity even at concentrations as high as 2 mM.[20]

The set of AuNPs **1–10** was initially tested as GALNS inhibitors at 0.2 mg mL^{-1} concentration in extracts from a pool of human leukocytes isolated from healthy donors, as previously reported.[18–20]

The collected data are summarized in Table 1. Homoligand glyco-AuNPs **1–4** showed percentages of inhibition higher than 75%, thus establishing them as promising GALNS inhibitors. For this reason, the corresponding IC$_{50}$ values (concentration of the inhibitor required for 50% inhibition of enzyme activity) were evaluated by measuring human enzyme activity at different glyco-AuNP concentrations (see Fig. S16†). Among these AuNPs, 100% βGal (βGal-Au (**2**), Fig. 3) was the best inhibitor (IC$_{50}$ = 9 µg mL^{-1}, 11 µM in terms of βGal concentration), while 100% αGal (αGal-Au (**3**), Fig. 3) showed one order of magnitude lower inhibition power (IC$_{50}$ = 140 µg mL^{-1}, 194 µM in terms of αGal). The same behaviour was observed for 100% αMan (αMan-Au (**4**), Fig. 3), which showed IC$_{50}$ = 120 µg mL^{-1} (175 µM in terms of αMan).

Importantly, the disulfide dimers (βGalC$_5$S)$_2$ **IVb** and (αManC$_5$S)$_2$ **IVd** did not show inhibitory activity towards GALNS when screened at 1 mM (see the ESI†). The significant inhibition observed for glyco-AuNPs **1–4** confirms that GALNS is particularly prone to accept multivalent ligands.

Since GALNS is a sulfatase, we envisaged that insertion of a sulfate component might have a synergistic effect with the sugar, thereby enhancing the inhibitory activity of the AuNPs. However, the experimental results indicated that the presence of the sulfated ligand in AuNPs **7–9** (50% sugar/50% sulfated ligand) did not affect the inhibitory potency with respect to the corresponding 100% glyco-AuNPs **1–3**. In particular, in terms of the βGal ligand, the IC$_{50}$ values were very close: 11 µM vs. 9 µM for AuNPs **2** and **8**, respectively. Similarly, in terms of the βGlc ligand, the IC$_{50}$ values were 47 µM for AuNPs **1** and 84 µM for AuNPs **7**, which lie in the same order of magnitude. In the case of AuNPs that display αGal, while AuNPs **3** were weak inhibitors (IC$_{50}$ = 194 µM), AuNPs **9** achieved only 58% inhibition; thus, the IC$_{50}$ was not measured. Accordingly, the AuNPs **5** coated with the sulfated ligand, which do not display any sugar component, were not good inhibitors of GALNS (42% inhibition at 0.2 mg mL^{-1}). Reasonably, the percentage of inhibition of the control AuNPs **6** coated with the phosphate ligand was even lower (27%). These latter data indicate that neither the TEG moiety nor a negative charge other than sulfate contributes significantly to the enzyme inhibition.

However, a different behaviour was noticed with the αMan-functionalized AuNPs **4** and **10**. In this case, more than one order of magnitude increase in inhibitory power is observed
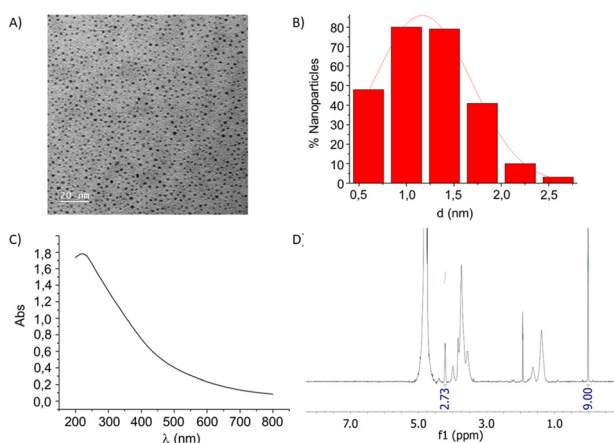
This journal is © The Royal Society of Chemistry 2023

Org. Biomol. Chem., 2023, **21**, 9362–9371 | **9365**

with AuNPs **10b** (IC_{50} = 7 μM) with respect to 100% αMan **4** (IC_{50} = 175 μM). The enhancement in the inhibitory activity seems to be related to the amount of sulfated ligand; in fact, AuNPs **10b** (50% sugar/50% sulfated ligand) are stronger inhibitors than AuNPs **10a** (80% sugar/20% sulfated ligand), which showed IC_{50} = 46 μM. In this case, the higher the sulfate amount, the higher the inhibitory power. This trend might be explained by the peculiar topology of presentation of the mannose ligand within these AuNPs.

Overall, the best inhibitors found in this work (AuNPs **2**, **8** and **10b**) have IC_{50} values in the same range as that of βGlc-Au-DAB-1 (Table 1) and even lower than that of the DAB-1 nonamer (Fig. 2B). Although the DAB-1 dimer and trimer (Fig. 2A) showed IC_{50} values in the low micromolar range, their syntheses required a multistep and time-consuming approach.

Among the best inhibitors, βGal-Au (**2**) was selected for further investigation being the simplest nanosystem to prepare. Thus, AuNPs **2** were also assayed towards the commercially available rhGALNS VIMIZIM® and an IC_{50} value very close to the one towards GALNS from the leukocyte homogenate (7 *vs.* 11 μM; Fig. S17†) was obtained.

The action mechanism of AuNPs **2** was determined by studying the dependence of the main kinetic parameters (K_m and V_{max}) on the inhibitor concentration. We observed that the K_m value remained constant, while the V_{max} value decreases with increasing inhibitor concentrations. This behaviour is in agreement with a non-competitive GALNS inhibitor (K_i = 0.76 ± 0.01 μg mL^{-1}; Fig. S20†).

In addition, an assessment of the ability of AuNPs **2** to stabilize GALNS against thermal denaturation was performed. rhGALNS VIMIZIM® was preincubated with 0, 0.001, 0.01, and 0.1 mg mL^{-1} AuNPs **2** before being heated at 48 °C for 40 and 60 min.

Untreated GALNS lost most of its activity under these conditions, with only 35% activity remaining after 1 h of heating (Fig. 5 and, for more details, see also Fig. S21†). Conversely, GALNS activity was retained by the inclusion of AuNPs **2** at all
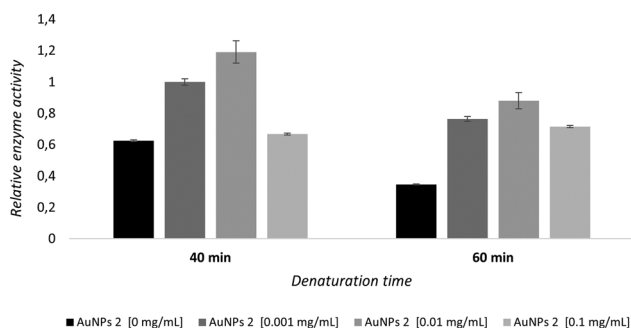
the investigated concentrations and time points (Fig. 5), suggesting that AuNPs **2** make the enzyme almost insensitive to thermal denaturation.

In particular, AuNPs **2** showed the best 1.73 and 1.26 stabilization ratios (defined as the ratios of inhibitor *vs.* control activity) at 0.001 mg mL^{-1} concentration at 40 and 60 min heating times, respectively (Fig. S23†). These data are remarkable since the highest stabilization is observed at a 6-fold lower concentration than the IC_{50} value (1 μg mL^{-1} *vs.* 6 μg mL^{-1}) of AuNPs **2**.

SAXS experiments

To have a direct proof of the association of βGal-Au (**2**) with GALNS, we conducted SAXS experiments. SAXS allows the measurement of the increase in the size of the nanoparticles due to the binding of GALNS. SAXS measurements on βGal-Au (**2**) were performed in the absence and presence of GALNS, in order to investigate the possible interaction between the AuNPs and the enzyme (Fig. 6). The SAXS fingerprint of GALNS in solution has also been obtained (data not shown), confirming its dimeric structure, in accordance with the computed scattering curve for the crystallographic human GALNS structure (PDB ID 4FDI).[14]

AuNPs **2** have a gold core, covered by an organic shell of different electron density; hence, SAXS experimental data (green points in Fig. 6) were successfully fitted by a core–shell model[29] using the GENFIT software.[30] Au electron density and β-D-galactoside-coating electron density were used to adequately fit experimental data; further details concerning this approach can be found in the literature.[31] The gold core diameter has been fitted considering its polydispersion (in agreement with TEM data, Fig. S5†), while the organic shell thickness has been considered as a monodisperse parameter. The diameter of AuNPs **2** determined by SAXS extends until ≈1.5 nm, and the AuNP core diameter shows a 10% polydispersion, similar to that found by TEM (Fig. S5†). The SAXS curve corresponding to AuNPs **2** in the presence of GALNS in
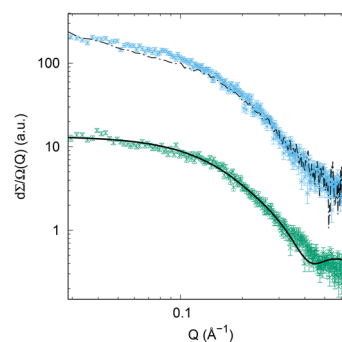

Fig. 5 Stabilization of rhGALNS Vimizim® evaluated *in vitro* by using heat inactivation. Relative enzymatic activity after thermal denaturation (48 °C) for 40 min and 60 min at the indicated inhibitor concentrations (mg mL^{-1}) with respect to the corresponding assay at 37 °C. Data for control are obtained as above except that no inhibitor is present (AuNPs **2** at 0 mg mL^{-1}).

Fig. 6 SAXS data corresponding to βGal-Au (**2**) at 1 mg mL^{-1} concentration (green points) and to the same AuNPs at 0.75 mg mL^{-1} concentration in the presence of 0.2 mg mL^{-1} GALNS (cyan points). The black continuous line is the theoretical fit obtained by a core−shell model. The black dashed line corresponds to the theoretical curve obtained by the weighted sum of the SAXS curves of the components of the mixture. The green and cyan points are shifted for clarity.

9366 | *Org. Biomol. Chem.*, 2023, **21**, 9362–9371

This journal is © The Royal Society of Chemistry 2023

solution is represented by the cyan points in Fig. 6. Based on the nominal concentrations of nanoparticles and enzymes in solution, we calculated the weighted sum of SAXS signals corresponding to AuNPs **2** and to GALNS and obtained the black dashed line shown in Fig. 6. If no interaction took place between nanoparticles and the enzyme, the experimental curve should exactly overlap with the dashed black line. However, it is clear that this theoretical curve is different from the experimental one (cyan points), providing evidence of an interaction of nanoparticles with the enzyme. In particular, the difference between the two curves at intermediate Q-values suggests a form factor change due to a structural arrangement that involves the enzyme and the nanoparticle.

Conclusions

In search for potential stabilizers of the enzyme GALNS, which could improve the ERT for Morquio A, a series of AuNPs decorated with different monosaccharides and/or anionic-ending (sulfate or phosphate) ligands were prepared and assayed as GALNS inhibitors. From a preliminary screening, the presence of the sulfated ligands on the AuNPs seems to slightly affect their inhibitory potency towards GALNS and a different behaviour depending on the sugar moieties and their C-1 configuration was observed. Although this latter aspect needs to be further investigated, the simple βGal-Au (**2**) emerged as a promising nanosystem and has been further tested, showing a non-competitive behaviour as well as the capability to restore the enzyme activity after thermal denaturation. The interaction between AuNPs **2** and the GALNS enzyme was also confirmed by SAXS experiments.

Due to the recent implications of GALNS in different pathologies other than LSDs, such as cancer and neuropathic pain, the development of novel multivalent nanosystems able to interact with this enzyme is of great interest towards alternative and/or multiple therapies. Further investigations are underway in our laboratories in this direction.

Experimental

General

Commercial reagents were used as received. All reactions were carried out under magnetic stirring. ^{1}H NMR spectra were recorded on a Varian Mercury-400 or on a Varian INOVA 400 instrument at 25 °C. Chemical shifts are reported relative to D$_2$O (^{1}H: δ = 4.79 ppm). The following abbreviations were used to designate multiplicities: m = multiplet and br = broad. Integrals are in accordance with assignments.

UV/vis spectra were recorded using a Varian Cary Win 4000 UV/Vis spectrophotometer. TEM analysis was performed using a JEOL JEM-2100F microscope, operating at 200 kV. UV/vis spectra were recorded using a Varian Cary Win 4000 UV/vis spectrophotometer. SAXS experiments were performed at the Austrian beamline at Elettra Synchrotron in Trieste, Italy.

Scattering patterns were recorded using the Pilatus 3 1 M detector system (Dectris, Switzerland). Elemental analyses were performed using a Thermoscientific FlashSmart Elemental Analyzer CHNS/O.

The syntheses of the thiol-ending β-D-glucoside **IVa**, β-D-galactoside **IVb**, α-D-galactoside **IVc**, α-D-mannoside **IVd**, phosphate ligand **V**, and sulfated ligand **VI** are described in the ESI.†

General procedure for the preparation of mixed-ligand gold nanoparticles glycoC$_5$S-Au-OSO$_3$$^-$. An aqueous solution of HAuCl$_4$ (25 mM, 1 equiv.) was added to a suitable mixture of thiol-ending ligands (3 equiv. overall) in H$_2$O/CH$_3$OH/CH$_3$COOH (3 : 3 : 1). An aqueous solution of NaBH$_4$ (1 M, 27 equiv.) was then portion-wise added under magnetic stirring. The black suspension formed was stirred for 2 hours at 25 °C. The solvent was evaporated at reduced pressure and the residue was washed with EtOH. The combined organics were evaporated and analysed by ^{1}H NMR. The residue was dissolved in a minimal volume of HPLC gradient grade water and purified by dialysis (SnakeSkin® Pleated Dialysis Tubing, 3500 MWCO). All the AuNPs were obtained as a dark-brown powder after freeze-drying and characterized *via* ^{1}H NMR, UV-vis spectroscopy, TEM, elemental analysis and qNMR. The values of the sulfate ligand **VI** content determined by qNMR are reported for a weighted amount of AuNPs. For the same amount of AuNPs, the sulfate ligand **VI** content was calculated using the average molecular weight estimated by combining TEM and elemental analyses.

50% βGlc-Au-OSO$_3$$^-$ (7).[26] Starting from a 1 : 1 mixture of compound **VI** (10 mg, 20.8 μmol) and βGlcC$_5$S **IVa** (5.9 mg, 20.8 μmol), HAuCl$_4$ (363 μL, 25 mM) and NaBH$_4$ (186 μL, 1 M), NPs **7** were obtained as a brown amorphous powder (3.5 mg, 88% yield). TEM (average diameter): 2.2 ± 0.4 nm; ^{1}H NMR (400 MHz, D$_2$O): 4.36 (br signal, 1H, *anomeric*), 4.13 (br signal, 2H, –CH_2OSO$_3$$^-$), 3.96–3.14 (br m, 24H, 3× –OCH_2CH$_2$O–, 3× –OCH_2–, H-2, H-3, H-4, H-5, H-6), 1.78–1.06 (br m, 24H, 12× –CH_2–); q^{1}H NMR (400 MHz, D$_2$O containing 0.05 wt% of 3-(trimethylsilyl)propionic-2,2,3,3-d$_4$ acid, sodium salt as internal standard): 1.63 mg of **7** contain 1.24 μmoles of sulfated ligand **VI**. Significant peaks: δ = 4.13 (br signal, 2H, –CH_2OSO$_3$$^-$), 0.02 (s, 9H, Si(C$H_3$)$_3$); δ UV-vis (H$_2$O, 0.1 mg mL^{-1}): no SPR peak observed; elemental analysis found (%): C 25.32, H 4.54, S 6.34; calc. for Au$_{201}$(C$_{19}$H$_{38}$O$_8$S$_2$Na)$_{60}$(C$_{11}$H$_{21}$O$_6$S)$_{60}$: C 25.32, H 4.18, S 6.76; average molecular weight: 85 kDa; estimated sulfated ligand content for 1.63 mg of AuNPs **7**: 1.15 μmoles.

50% βGal-Au-OSO$_3$$^-$ (8). Starting from a 1 : 1 mixture of compound **VI** (6.0 mg, 12.5 μmol) and βGalC$_5$S (**IVb**) (3.52 mg, 12.5 μmol), HAuCl$_4$ (219 μL, 25 mM) and NaBH$_4$ (112 μL, 1 M), NPs **8** were obtained as a brown amorphous powder (1.4 mg, 58% yield). TEM (average diameter): 1.2 ± 0.4 nm; ^{1}H NMR (400 MHz, D$_2$O): δ 4.41 (br signal, 1H, *anomeric*), 4.21 (br signal, 2H, –CH_2OSO$_3$$^-$), 3.99–3.55 (br m, 22H, 3× –OCH_2CH$_2$O–, 2× –OCH_2–, H-2, H-3, H-4, H-5, H-6), 2.08–1.19 (br m, 24H, 12× –CH_2–); q^{1}H NMR (400 MHz, D$_2$O containing 0.05 wt% of 3-(trimethylsilyl)propionic-2,2,3,3-d$_4$ acid, sodium

This journal is © The Royal Society of Chemistry 2023

Org. Biomol. Chem., 2023, **21**, 9362–9371 | **9367**

salt as internal standard): 0.5 mg of **8** contain 0.18 µmoles of sulfated ligand **VI**. Significant peaks: δ = 4.21 (br signal, 2H, $-CH_2OSO_3^-$), 0.02 (s, 9H, $Si(CH_3)_3$); UV-Vis (H_2O, 0.2 mg mL^{-1}): no SPR peak observed; elemental analysis found (%): C 13.91, H 2.18, S 3.41; calc. for $Au_{140}(C_{19}H_{38}O_8S_2Na)_{15}(C_{11}H_{21}O_6S)_{15}$: C 13.85, H 2.29, S 3.70; average molecular weight: 39 kDa; estimated sulfated ligand content for 0.5 mg of AuNPs **8**: 0.19 µmoles.

50% αGal-Au-OSO$_3^-$ (9). Starting from a 1 : 1 mixture of compound **VI** (6.0 mg, 12.5 µmol) and αGalC$_5$S (**IVc**) (3.52 mg, 12.5 µmol), HAuCl$_4$ (186 µL, 25 mM) and NaBH$_4$ (95.4 µL, 1 M), NPs **9** were obtained as a brown amorphous powder (1.9 mg, 93% yield). TEM (average diameter): 1.4 ± 0.3 nm; ^{1}H NMR (400 MHz, D_2O): δ Anomeric proton presumably hidden under the HDO/H_2O signal, 4.14 (br signal, 2H, $-CH_2OSO_3^-$), 4.06–3.35 (br m, 22H, 3× $-OCH_2CH_2O-$, 2× $-OCH_2-$, H-2, H-3, H-4, H-5, H-6), 2.10–1.22 (br m, 24H, 12× $-CH_2-$); UV-vis (H_2O, 0.2 mg mL^{-1}): no SPR peak observed; elemental analysis found (%): C 25.32, 4.54, S 6.34; calc. for $Au_{140}(C_{19}H_{38}O_8S_2Na)_{41}(C_{11}H_{21}O_6S)_{41}$: C 25.10, H 4.14, S 6.70; average molecular weight: 58 kDa.

80% αMan-Au-OSO$_3^-$ (10a). Starting from a 1 : 4 mixture of compound **VI** (2.9 mg, 6.20 µmol) and αManC$_5$S (**IVd**) (7.0 mg, 24.9 µmol), HAuCl$_4$ (412 µL, 25 mM) and NaBH$_4$ (279 mL, 1 M), NPs **10a** were obtained as a brown amorphous powder (4.4 mg, quantitative yield). TEM (average diameter): 1.5 ± 0.4 nm; ^{1}H NMR (400 MHz, D_2O): δ Anomeric proton presumably hidden under the HDO/H_2O signal; 4.20 (br signal, 2H, $-CH_2OSO_3^-$), 3.91–3.55 (br m, ≈26H), 2.02–1.11 (br m, ≈30H); q^{1}H NMR (400 MHz, D_2O containing 0.05 wt% of 3-(trimethyl-silyl)propionic-2,2,3,3-d$_4$ acid, sodium salt as an internal standard): 1.40 mg of **10a** contain 0.32 µmoles of sulfated ligand **VI**. Significant peaks: δ = 4.20 (br s, 2H, $-CH_2OSO_3^-$), 0.00 (s, 9H, $Si(CH_3)_3$); UV-Vis (H_2O, 0.2 mg mL^{-1}): no SPR peak observed; elemental analysis found (%): C 17.31, H 2.78, S 4.63; calc. for $Au_{140}(C_{19}H_{38}NaO_8S_2)_{10}(C_{11}H_{21}O_6S)_{40}$: C 17.34, H 2.82, S 4.41; average molecular weight: 44 kDa; estimated sulfated ligand content for 1.4 mg of AuNPs **10a**: 0.32 µmoles.

50% αMan-Au-OSO$_3^-$ (10b). Starting from a 1 : 1 mixture of compound **VI** (11.7 mg, 24.8 µmol) and αManC$_5$S (**IVd**) (7.0 mg, 24.9 µmol), HAuCl$_4$ (660 µL, 25 mM) and NaBH$_4$ (446 µL, 1 M), NPs **10b** were obtained as a brown amorphous powder (3.2 mg, 43% yield). TEM (average diameter): 2.0 ± 0.4 nm; ^{1}H NMR (400 MHz, D_2O): δ Anomeric proton presumably hidden under HDO/H_2O signal; 4.20 (br signal, 2H, $-CH_2OSO_3^-$), 3.91–3.55 (br m, 3× $-OCH_2CH_2O-$, 2× $-OCH_2-$, H-2, H-3, H-4, H-5, H-6), 2.02–1.11 (br m, 24H, 12× $-CH_2-$); q^{1}H NMR (400 MHz, D_2O containing 0.05 wt% of 3-(trimethyl-silyl)propionic-2,2,3,3-d$_4$ acid, sodium salt as an internal standard): 1.40 mg of **10b** contain 0.63 µmoles of sulfated ligand **VI**. Significant peaks: δ = 4.20 (br s, 2H, $-CH_2OSO_3^-$), 0.00 (s, 9H, $Si(CH_3)_3$); UV-vis (H_2O, 0.2 mg mL^{-1}): no SPR peak observed; elemental analysis found (%): C 17.34, 2.92, S 4.93; calc. for $Au_{201}(C_{11}H_{21}O_6S)_{30}(C_{19}H_{38}O_8S_2Na)_{30}$: C 17.30, H 2.86, S 4.62; average molecular weight: 62 kDa; estimated sulfated ligand content for 1.40 mg of AuNPs **10b**: 0.67 µmoles.

Biological evaluation

Enzymatic assays towards human GALNS in leukocytes isolated from healthy donors. All experiments on biological materials were performed in accordance with the ethical standards of the institutional research committee and with the 1964 Helsinki Declaration and its later amendments. In keeping with ethical guidelines, all blood and cell samples were obtained for storage and analysed only after written informed consent of the patients (and/or their family members) was obtained, using a form approved by the local Ethics Committee (Assigned code: Lysolate "Late-onset Lysosomal Storage Disorders (LSDs) in the differential diagnosis of neurodegenerative diseases: development of new diagnostic procedures and focus on potential pharmacological chaperones (PCs)." Project ID code: 16774_bio, 5 May 2020, Comitato Etico Regionale per la Sperimentazione Clinica della Regione Toscana, Area Vasta Centro, Florence, Italy). Control and patient samples were anonymized and used only for research purposes.

A preliminary biological screening of compounds **IVb** and **IVd** at 1 mM (as disulfides), AuNPs **1–5** and **7–10** at 0.2 mg mL^{-1} inhibitor concentration and AuNPs **6** at 0.1 mg mL^{-1} inhibitor concentration was performed towards GALNS in leukocytes isolated from healthy donors (controls).

Isolated leukocytes were disrupted by sonication, and a micro BCA protein assay kit (Sigma–Aldrich) was used to determine the total protein amount for the enzymatic assay, according to the manufacturer instructions. Enzyme activity was measured by setting up the reaction in 0.2 mL tubes and performing the experiments in triplicate as follows.

AuNP solution (3 µL), 4.29 µg µL^{-1} leukocyte homogenate 1 : 5 (7 µL) and 20 µL of 4-methylumbelliferyl-β-galactoside-6-sulfate·Na substrate solution (6.66 mM) in Na-acetate/acetic acid buffer (0.1 M/0.1 M, pH 4.3) containing 0.1 M NaCl, 0.02% (w/v) NaN$_3$ and 5 mM Pb-acetate were incubated for 17 h at 37 °C. After step one, the tubes were placed on an ice cooler and the reaction was stopped by addition of 5 µL of Na-phosphate buffer (0.9 M, pH 4.3) containing 0.02% (w/v) of NaN$_3$ and by efficient mixing using a vortex. Then, 10 µL of β-Gal-A-10U were added to each sample and samples were incubated for 2 h at 37 °C. At the end of this period the tubes were placed on an ice cooler and the samples were transferred to a cooled flat-bottomed 96 well plate, and the reaction was immediately stopped with 200 µL of NaHCO$_3$/Na$_2$CO$_3$ buffer (0.5 M/0.5 M pH 10.7) containing 0.025% (w/v) of Triton X-100. Fluorescence was measured using a SpectraMax M2 microplate reader (Molecular-Devices) with a 365 nm excitation wavelength and a 435 nm emission wavelength. The percentage of GALNS inhibition was given with respect to the control (without compound). Experiments were performed in triplicate, and the mean ± S.D. was calculated.

IC$_{50}$ determination. The IC$_{50}$ values of inhibitors against human GALNS in leukocytes isolated from healthy donors or against recombinant human GALNS (rhGALNS VIMIZIM®) were determined by measuring the initial hydrolysis rate with

9368 | *Org. Biomol. Chem.*, 2023, **21**, 9362–9371

This journal is © The Royal Society of Chemistry 2023

4-methylumbelliferyl-β-galactoside-6-sulfate·Na (6.66 mM) at different concentrations of inhibitors (concentration range from 10^{-4} mg mL^{-1} to 0.2 mg mL^{-1}). Data obtained were fitted by using the appropriate equation (for more details and IC$_{50}$ curves, see the ESI†).

Stabilization of recombinant GALNS under thermal denaturation conditions. The thermal stability induced by AuNPs **2** against rhGALNS VIMIZIM® (1.0×10^{-5} mg mL^{-1}) was determined by measuring the hydrolysis rate with 4-methylumbelliferyl-β-galactoside-6-sulfate·Na (6.66 mM) after denaturation of the enzyme at 48 °C for 40 minutes or 60 minutes with or without (Ctrl) different concentrations (0.001 mg mL^{-1}, 0.01 mg mL^{-1}, 0.1 mg mL^{-1}, and 0.2 mg mL^{-1}) of AuNPs **2**.

AuNPs **2** (3 μL) and rhGALNS (7 μL) were incubated for 20 minutes in an ice bath and then for 0 minutes, 40 minutes or 60 minutes at 48 °C.

After incubation 20 μL of the 4-methylumbelliferyl-β-galactoside-6-sulfate·Na substrate solution in Na-acetate/acetic acid buffer (0.1 M/0.1 M, pH 4.3) containing 0.1 M NaCl, 0.02% (w/v) NaN$_3$ and 5 mM Pb-acetate was added. The tubes were incubated for 17 h at 37 °C. After this first incubation the tubes were placed on an ice cooler and the reaction was stopped by addition of 5 μL of Na-phosphate buffer (0.9 M, pH 4.3) containing 0.02% (w/v) of NaN$_3$ and by efficient mixing using a vortex. Then, 10 μL of β-Gal-A-10U were added to each sample and samples were incubated for 2 h at 37 °C. After this, the tubes were placed on an ice cooler and the samples were transferred to a cooled flat-bottomed 96 well plate, and the reaction was immediately stopped with 200 μL of NaHCO$_3$/Na$_2$CO$_3$ buffer (0.5 M/0.5 M pH 10.7) containing 0.025% (w/v) of Triton X-100. Fluorescence was measured using a SpectraMax M2 microplate reader (Molecular-Devices) with a 365 nm excitation wavelength and a 435 nm emission wavelength.

Experiments were performed in triplicate, and the mean ± S.D. was calculated.

SAXS experiments. AuNPs at 1 mg mL^{-1} (200 μL) in Milli-Q water without the enzyme were measured as a control. AuNPs at 0.75 mg mL^{-1} were incubated for 17 hours at room temperature with 0.2 mg mL^{-1} GALNS in a final volume of 200 μL of Milli-Q water. Detector images were radially averaged, obtaining the scattering intensity as a function of the magnitude of the scattering vector Q defined as: $Q = (4\pi\sin(\theta))/\lambda$, where 2θ is the scattering angle and λ is the X-ray wavelength, which is 0.154 nm. Further details on the data reduction procedure can be found in the literature.[31]

Author contributions

FB, CV, CC and AB carried out the syntheses of the ligands and gold nanoparticles, as well as their characterization, under the guidance of CM and MM. FB and CV wrote the ESI† with the support of SEM, CM and MM. FCl performed the biological tests and analysed the data with the supervision of PP and AM. PA and MGO performed the SAXS measurements and further analysed the data with the help of SEM. CM and MM conceived and supervised the research and with FCa wrote the manuscript. AG, MGO, and SEM critically revised the initial draft of the manuscript. All authors have read and agreed to the published version of the manuscript.

Conflicts of interest

There are no conflicts of interest to declare.

Acknowledgements

References

1 (a) F. M. Platt, A. D'Azzo, B. L. Davidson, E. F. Neufeld and C. J. Tifft, *Nat. Rev. Dis. Primers*, 2018, **4**, 27; (b) A. R. A. Marques and P. Saftig, *J. Cell Sci.*, 2019, **132**, jcs221739; (c) G. Parenti, G. Andria and A. Ballabio, *Annu. Rev. Med.*, 2015, **66**, 471–486; (d) S. Ortolano, I. Viéitez, C. Navarro and C. Spuch, *Recent Pat. Endocr., Metab. Immune Drug Discovery*, 2014, **8**, 9–25.

2 (a) L. Liguori, M. Monticelli, M. Allocca, B. Hay Mele, J. Lukas, M. V. Cubellis and G. Andreotti, *Int. J. Mol. Sci.*, 2020, **21**, 489; (b) E. M. Sánchez-Fernández, J. M. García

This journal is © The Royal Society of Chemistry 2023

Org. Biomol. Chem., 2023, **21**, 9362–9371 | **9369**

Fernández and C. Ortiz Mellet, *Chem. Commun.*, 2016, **52**, 5497–5515; (*c*) R. E. Boyd, G. Lee, P. Rybczynski, E. R. Benjamin, R. Khanna, B. A. Wustman and K. J. Valenzano, *J. Med. Chem.*, 2013, **56**, 2705–2725; (*d*) M. Martínez-Bailén, F. Clemente, C. Matassini and F. Cardona, *Pharmaceuticals*, 2022, **15**, 823.

3 (*a*) D. M. Pereira, P. Valentão and P. B. Andrade, *Chem. Sci.*, 2018, **9**, 1740–1752; (*b*) M. Convertino, J. Das and N. V. Dokholyan, *ACS Chem. Biol.*, 2016, **11**, 1471–1489.

4 (*a*) E. H. McCaerty and L. J. Scott, *Drugs*, 2019, **79**, 543–554; (*b*) N. Moran, *Nat. Biotechnol.*, 2018, **36**, 913.

5 (*a*) L. Morquio, *Arch. Med. Enfants*, 1929, **32**, 129; (*b*) M. F. Algahim and G. H. Almassi, *Ther. Clin. Risk Manage.*, 2013, **9**, 45–53; (*c*) G. A. Solanki, K. W. Martin, M. C. Theroux, C. Lampe, K. K. White, R. Shediac, C. G. Lampe, M. Beck, W. G. Mackenzie, C. J. Hendriksz and P. R. Harmatz, *J. Inherited Metab. Dis.*, 2013, **36**, 339–355; (*d*) K. Sawamoto, J. V. A. Gonzalez, M. Piechnik, F. J. Otero, M. L. Couce, Y. Suzuki and S. Tomatsu, *Int. J. Mol. Sci.*, 2020, **21**, 1517.

6 H. Peracha, K. Sawamoto, L. Averill, H. Kecskemethy, M. Theroux, M. Thacker, K. Nagao, C. Pizarro, W. Mackenzie, H. Kobayashi, S. Yamaguchi, Y. Suzuki, K. Orii, T. Orii, T. Fukao and S. Tomatsu, *Mol. Genet. Metab.*, 2018, **125**, 18–37.

7 K. Haddley, *Drugs Today*, 2014, **50**, 475–483.

8 (*a*) R. Khanna, J. J. Flanagan, J. Feng, R. Soska, M. Frascella, L. J. Pellegrino, Y. Lun, D. Guillen, D. J. Lockhart and K. J. Valenzano, *PlosOne*, 2012, **7**, e40776; (*b*) J.-S. Shen, N. J. Edwards, Y. B. Hong and G. J. Murray, *Biochem. Biophys. Res. Commun.*, 2008, **369**, 1071–1075; (*c*) C. Porto, M. Cardone, F. Fontana, B. Rossi, M. R. Tuzzi, A. Tarallo, M. V. Barone, G. Andria and G. Parenti, *Mol. Ther.*, 2009, **17**, 964–971; (*d*) E. R. Benjamin, R. Khanna, A. Schilling, J. J. Flannagan, L. J. Pellegrino, N. Brignol, Y. Lun, D. Guillen, B. E. Ranes, M. Frascella, R. Soska, J. Feng, L. Dungan, B. Young, D. J. Lockhart and K. J. Valenzano, *Mol. Ther.*, 2012, **20**, 717–726.

9 C. J. Alméciga, O. A. Hidalgo, S. Olarte-Avellaneda, A. Rodríguez-López, E. Guzman, R. Garzón, L. N. Pimentel-Vera, M. A. Puentes-Tellez, A. F. Rojas-Rodriguez, K. Gorshkov, R. Li and W. Zheng, *J. Med. Chem.*, 2019, **62**, 6175–6189.

10 S. Olarte-Avellaneda, J. Cepeda Del Castillo, A. F. Rojas-Rodriguez, O. Sánchez, A. Rodríguez-López, D. A. Suárez García, L. M. Salazar Pulido and C. J. Alméciga-Díaz, *ACS Med. Chem. Lett.*, 2020, **11**, 1377–1385.

11 J. C. Losada Díaz, J. Cepeda del Castillo, E. A. Rodriguez-López and C. J. Alméciga- Díaz, *Int. J. Mol. Sci.*, 2020, **21**, 232.

12 S. Bhattacharyya, L. Feferman and J. K. Tobacman, *Prostate*, 2019, **79**, 689–700.

13 C. E. Müller and T. Claff, *Signal Transduction Targeted Ther.*, 2022, **7**, 333.

14 Y. Rivera-Colón, E. K. Schutsky, A. Z. Kita and S. C. Garman, *J. Mol. Biol.*, 2012, **423**, 736–751.

15 S. Cecioni, A. Imberty and S. Vidal, *Chem. Rev.*, 2015, **115**, 525–561.

16 (*a*) P. Compain and A. Bodlenner, *ChemBioChem*, 2014, **15**, 1239–1251; (*b*) S. G. Gouin, *Chem. – Eur. J.*, 2014, **20**, 11616–11628; (*c*) R. Zelli, J.-F. Longevial, P. Dumy and A. Marra, *New J. Chem.*, 2015, **30**, 5050–5074; (*d*) N. Kanfar, E. Bartolami, R. Zelli, A. Marra, J.-Y. Winum, S. Ulrich and P. Dumy, *Org. Biomol. Chem.*, 2015, **13**, 9894–9906; (*e*) C. Matassini, C. Parmeggiani, F. Cardona and A. Goti, *Tetrahedron Lett.*, 2016, **57**, 5407–5415; (*f*) P. Compain, *Chem. Rec.*, 2020, **20**, 10–22.

17 (*a*) M. Mammen, S.-K. Choi and G. M. Whitesides, *Angew. Chem., Int. Ed.*, 1998, **37**, 2754–2794; (*b*) L. L. Kiessling, J. E. Gestwicki and L. E. Strong, *Curr. Opin. Chem. Biol.*, 2000, **4**, 696–703; (*c*) *Synthetic Multivalent Molecules: Concepts and Biomedical Applications*, ed. S.-K. Choi, Wiley, New Jersey, 2004; (*d*) M. González-Cuesta, C. Ortiz Mellet and J. M. García Fernández, *Chem. Commun.*, 2020, **56**, 5207–5222.

18 C. Matassini, G. D'Adamio, C. Vanni, A. Goti and F. Cardona, *Eur. J. Org. Chem.*, 2019, 4897–4905.

19 G. D'Adamio, C. Matassini, C. Parmeggiani, S. Catarzi, A. Morrone, A. Goti, P. Paoli and F. Cardona, *RSC Adv.*, 2016, **6**, 64847–64851.

20 C. Matassini, C. Vanni, A. Goti, A. Morrone, M. Marradi and F. Cardona, *Org. Biomol. Chem.*, 2018, **16**, 8604–8612.

21 *Iminosugars: from Synthesis to Therapeutic Applications*, ed. P. Compain and O. R. Martin, Wiley VCH, New York, 2007.

22 (*a*) M. Marradi, F. Chiodo, I. García and S. Penadés, *Chem. Soc. Rev.*, 2013, **42**, 4728–4745; (*b*) M. Marradi, I. García and S. Penadés, *Biomater Science*, 2011, **104**, 141–173.

23 M. de la Fuente, A. G. Barrientos, T. C. Rojas, J. Rojo, J. Cañada, A. Fernández and S. Penadés, *Angew. Chem., Int. Ed.*, 2001, **40**, 2257–2261.

24 M. Brust, M. Walker, D. Bethell, D. J. Schiffrin and R. Whyman, *J. Chem. Soc., Chem. Commun.*, 1994, 801–802.

25 (*a*) O. Martínez-Ávila, K. Hijazi, M. Marradi, C. Clevel, C. Campion, C. Kelly and S. Penadés, *Chem. – Eur. J.*, 2009, **15**, 9874–9888; (*b*) A. Irure, M. Marradi, B. Arnáiz, N. Genicio, D. Padro and S. Penadés, *Biomater. Sci.*, 2013, **1**, 658–668.

26 P. Di Gianvincenzo, M. Marradi, O. M. Martínez-Ávila, L. M. Bedoya, J. Alcamí and S. Penadés, *Bioorg. Med. Chem. Lett.*, 2010, **20**, 2718–2721.

27 M. J. Hostetler, J. E. Wingate, C.-J. Zhong, J. E. Harris, R. W. Vachet, M. R. Clark, J. D. Londono, S. J. Green, J. J. Stokes, G. D. Wignall, G. L. Glish, M. D. Porter, N. D. Evans and R. W. Murray, *Langmuir*, 1998, **14**, 17–30.

28 (*a*) F. Manea, C. Bindoli, S. Fallarini, G. Lombardi, L. Polito, L. Lay, R. Bonomi, F. Mancin and P. Scrimin, *Adv. Mater.*, 2008, **20**, 4348–4352; (*b*) C. Matassini, M. Marradi, F. Cardona, C. Parmeggiani, I. Robina, A. J. Moreno-Vargas, S. Penadés and A. Goti, *RSC Adv.*, 2015, **5**, 95817–95822; (*c*) F. Chiodo, P. M. Enríquez-Navas, J. Angulo, M. Marradi and S. Penadés, *Carbohydr. Res.*, 2015, **405**, 102–109.

9370 | *Org. Biomol. Chem.*, 2023, **21**, 9362–9371

This journal is © The Royal Society of Chemistry 2023

29 I. Berndt, J. S. Pedersen and W. Richtering, *J. Am. Chem. Soc.*, 2005, **127**, 9372–9373.

30 F. Spinozzi, C. Ferrero, M. G. Ortore, A. De Maria Antolinos and P. Mariani, *J. Appl. Crystallogr.*, 2014, **47**, 1132–1139.

31 P. Andreozzi, C. Simó, P. Moretti, J. Martinez Porcel, T. U. Lüdtke, M. d. l. A. Ramirez, L. Tamberi, M. Marradi, H. Amenitsch, J. Llop, M. G. Ortore and S. E. Moya, *Small*, 2021, **17**, 2102211.

This journal is © The Royal Society of Chemistry 2023

Org. Biomol. Chem., 2023, **21**, 9362–9371 | **9371**